Catalabolism of lysosome-related organelles in color-changing spiders supports intracellular turnover of pigments

Florent Figon[a,1,2], Ilse Hurbain[b,c], Xavier Heiligenstein[d], Sylvain Trépout[e], Arnaud Lanoue[f], Kadda Medjoubi[g], Andrea Somogyi[g], Cédric Delevoye[b,c], Graça Raposo[b,c], and Jérôme Casas[a,1]

[a]Institut de Recherche sur la Biologie de l'Insecte, CNRS UMR 7261, Université de Tours, 37200 Tours, France; [b]Institut Curie, CNRS UMR 144, Structure and Membrane Compartments, Paris Sciences & Lettres (PSL) Research University, 75005 Paris, France; [c]Institut Curie, CNRS UMR 144, Cell and Tissue Imaging Facility (Plateforme d'Imagerie Cellulaire et Tissulaire, Infrastructures en Biologie, Santé et Agronomie [PICT-IBiSA]), PSL Research University, 75005 Paris, France; [d]CryoCapCell, 94276 Le Kremlin-Bicêtre, France; [e]Institut Curie, INSERM U1196, CNRS UMR 9187, Université Paris-Sud, Université Paris-Saclay, 91405 Orsay, France; [f]Biomolécules et Biotechnologies Végétales, Équipe d'Accueil 2106, Université de Tours, 37200 Tours, France; and [g]Synchrotron SOLEIL, 91192 Gif-sur-Yvette, France

Edited by Jennifer Lippincott-Schwartz, Janelia Farm Research Campus, Ashburn, VA, and approved July 14, 2021 (received for review February 23, 2021)

Pigment organelles of vertebrates belong to the lysosome-related organelle (LRO) family, of which melanin-producing melanosomes are the prototypes. While their anabolism has been extensively unraveled through the study of melanosomes in skin melanocytes, their catabolism remains poorly known. Here, we tap into the unique ability of crab spiders to reversibly change body coloration to examine the catabolism of their pigment organelles. By combining ultrastructural and metal analyses on high-pressure frozen integuments, we first assess whether pigment organelles of crab spiders belong to the LRO family and second, how their catabolism is intracellularly processed. Using scanning transmission electron microscopy, electron tomography, and nanoscale Synchrotron-based scanning X-ray fluorescence, we show that pigment organelles possess ultrastructural and chemical hallmarks of LROs, including intraluminal vesicles and metal deposits, similar to melanosomes. Monitoring ultrastructural changes during bleaching suggests that the catabolism of pigment organelles involves the degradation and removal of their intraluminal content, possibly through lysosomal mechanisms. In contrast to skin melanosomes, anabolism and catabolism of pigments proceed within the same cell without requiring either cell death or secretion/phagocytosis. Our work hence provides support for the hypothesis that the endolysosomal system is fully functionalized for within-cell turnover of pigments, leading to functional maintenance under adverse conditions and phenotypic plasticity. First formulated for eye melanosomes in the context of human vision, the hypothesis of intracellular turnover of pigments gets unprecedented strong support from pigment organelles of spiders.

endosome | pigment granule | melanosome | ommochrome | mimicry

How and why animals produce their colors are fundamental questions in biology. In cases where pigments are involved, they are usually synthesized and stored in specialized intracellular organelles (1). Bagnara et al. (2) postulated in 1979 that all pigment organelles of vertebrates derive from a common primordial organelle. Since then, an increasing body of evidence has shown that pigment organelles, from mammal melanosomes to snake pterinosomes, belong to the lysosome-related organelle (LRO) family (3, 4). LROs intersect the endolysosomal system (5), which forms a complex and active network of membrane-bound compartments produced by endocytic and secretory pathways (6). Studying the subcellular aspect of LROs in relation to pigmentation is therefore a critical step to understand animal coloration.

Detailed investigations of intracellular processes and trafficking leading to the biogenesis of pigment LROs have been largely performed on mammalian melanosomes (3, 5). They revealed that skin melanocytes divert components of the endolysosomal system to progressively generate melanosome precursors derived from endosomes, bearing intraluminal vesicles (ILVs) and amyloid fibrils, and then mature pigmented melanosomes that are transferred to keratinocytes. Melanosome formation is controlled by a range of genes involved in the endolysosomal system of mammals (3, 5). The finding of homologous genes controlling pterinosomes, iridisomes, and ommochromasomes of snakes and insects, among others, has led to a general model of pigment organelle formation (3, 4, 7). However, coloration involves not only pigmentation phases but also, bleaching phases that lead to pigment removal, a process that is far less understood, even for melanosomes (8).

While bleaching can result from death of pigment-containing cells, such as during peeling (9), this process is also compatible with pigment cells remaining alive (10). The latter phenomenon

Significance

Pigment–light interactions have shaped animal evolution, from vision to camouflage. How organisms cope with harmful photodegradative products while maintaining pigment-bearing cell integrity, from skin to light screening in eyes, remains mysterious. We studied color-changing crab spiders to unravel the intracellular mechanisms leading to within-cell formation and degradation of pigment organelles. We found that they belong to the widespread lysosome-related organelle family, like vertebrate melanosomes. The endolysosomal system allows reversible coloration in spiders by sustaining pigment turnover thanks to its fundamental anabolic and catabolic functions, a hypothesis first laid out for human eyes. Our findings imply that the ubiquitous endolysosomal system had been repurposed early in animal evolution to handle pigment–light interactions, providing phenotypic plasticity and cell function maintenance.

Author contributions: F.F., K.M., A.S., C.D., and J.C. designed research; F.F., I.H., X.H., S.T., and A.S. performed research; A.L. and G.R. contributed new reagents/analytic tools; F.F., I.H., X.H., S.T., A.L., K.M., A.S., C.D., G.R., and J.C. analyzed data; F.F. and J.C. conceptualized the question; F.F. and J.C. wrote the paper; and all authors edited versions of the paper.

The authors declare no competing interest.

This article is a PNAS Direct Submission.

[1]To whom correspondence may be addressed. Email: florent.figon@univ-tours.fr or jerome.casas@univ-tours.fr.

[2]Present address: Laboratoire d'Écologie Alpine, CNRS UMR 5553, Université Grenoble Alpes, Université Savoie Mont-Blanc, 38054 Grenoble, France.

This article contains supporting information online at https://www.pnas.org/lookup/suppl/doi:10.1073/pnas.2103020118/-/DCSupplemental.

Published August 25, 2021.

questions how pigment cells accommodate both the production and the removal of pigment organelles, as well as whether recycling pathways connecting the two phases exist. The occurrence of within-cell melanosomal degradation as a common physiological process required for melanin turnover has long been debated (8, 11–13). Here, turnover is defined as a pigmentation–depigmentation–repigmentation cycle at the cellular scale, without requiring the reuse of organellar materials. Evidence for physiological degradations of pigment LROs remains scarce [but see the studies on differences in human skin pigmentation (14, 15)], which we attribute to the rarity of biological systems displaying active and concomitant production and removal of pigments within a single cell and a lack of studies focusing on this phase.

Color-changing crab spiders can dynamically match the flower color on which they hunt (16, 17). They do so by reversibly changing their body coloration over the course of a few days, up to weeks, between white and yellow (18). This slow morphological color changes results from the metabolism of yellow pigments, thought to be ommochromes, in integument cells (10, 18, 19). Ommochromes are pigments deriving from tryptophan through the formation of colored kynurenines and transient precursors (7, 20). They are involved in various color-changing species, including dragonflies and cephalopods (21–23). The crab spider is the best understood nonmodel system among the ones displaying morphological color changes in terms of pigment organelle metabolism, ranging from locusts to planarians (24, 25). During yellowing (i.e., anabolic phase), pigments are deposited within specialized intracellular organelles, whose intracellular origin remains undetermined (19). During bleaching, pigment organelles are thought to undergo an autocatalytic process and to recycle their membrane for another cycle of yellowing (10). However, ultrastructural and chemical evidence for this recycling process is scarce, and we do not fully comprehend how both anabolism and catabolism of ommochromes and pigment organelles of crab spiders fit within intracellular trafficking pathways (7). Testing the hypothesis that these pigment organelles are members of the LRO family may help position them into the endolysosomal system, which in return, might provide insights into the roles of the endolysosomal system in both pigmentation and bleaching phases, as well as in reversibility.

LROs are defined as being morphologically distinct from lysosomes, containing a subset of cell type–specific contents necessary for their function and being in many instances secretory organelles. However, LROs also share features with lysosomes such as the presence of lysosomal-associated membrane proteins, hydrolases, and an acidic pH (at least temporary), and some can be accessible via the endocytic pathway (3, 5). In practice, the assignment of organelles to the LRO family is based on genetic defects associated with human diseases, such as Hermansky–Pudlak, Griscelli, and Chediak–Higashi syndromes (3–5). However, such genetic dependence cannot be tested in spiders because they are in most cases not genetically tractable. Therefore, other markers of their secretory/endocytic nature should be assessed. LROs often bear ultrastructural signatures of their intracellular origin, such as endosomal/Golgi connections, ILVs, physiological amyloid fibrils, and membrane tubulations (6). Conversely, LROs act as important regulators of metals by storing and releasing them in a dynamic manner (26). Specific techniques are required to retain such labile signatures as membrane tubulations and metals. For relatively thick tissues, this is best done by high-pressure freezing (HPF), which avoids artifacts produced by chemical fixatives (27). As an example, electron microscopy (EM) combined with HPF successfully revealed the morphological details of LROs like melanosomes (28) and Weibel–Palade bodies (29, 30) and their close contacts with other organelles (28). Given the submicrometer size of pigment organelles (19), detection of metals in their lumen can only be tackled by highly sensitive and spatially resolved nanoimaging methods (31), like scanning Synchrotron X-ray fluorescence (SXRF). SXRF is a state-of-the-art chemical imaging technique to map multiple trace elements with subpart per million sensitivity down to a few tens of nanometers resolution (32–34). Therefore, to reveal the intracellular origin of pigment organelles and their catabolism, we exploited the combination of EM and SXRF on white, yellow, and bleaching crab spiders fixed in a near-native state by HPF (*SI Appendix* discusses the overall fixation quality; *SI Appendix*, Fig. S1).

Results

Ultrastructure and Typology of Pigment Organelles in Relation to Coloration. From an ultrastructural point of view, pigment organelles of white and yellow spiders mainly differed by the density and the organization of their intraluminal materials (*SI Appendix*, Fig. S2). We classified pigment organelles preserved by HPF into six morphological types (Fig. 1*A*). The roundish a type, corresponding to precursor organelles described in previous studies (10, 19), is present in both white and yellow spiders, although it was the main pigment organelle type in white ones (*SI Appendix*, Table S1). HPF allowed us to describe their internal content, consisting of a diffuse fibrillary material (Fig. 1 *A*, *a*), with various stages of density (*SI Appendix*, Fig. S2*B*). The roundish b type, corresponding to the mature pigment organelles also previously described (10, 19), is fully packed with electron-dense materials (Fig. 1 *A*, *b*) and is predominant in yellow spiders (*SI Appendix*, Table S1), reflecting its high pigment content. Contrary to a and b types, c to f types are only observed in yellow spiders (*SI Appendix*, Table S1), and they are described here. The c type is an ovoid organelle characterized by several cores of variously dense materials forming pigment clusters of different natures (Fig. 1 *A*, *c*, arrowheads and *SI Appendix*, Table S1). The roundish d type possesses a dense crown of material and an electron-lucent center (Fig. 1 *A*, *d* and *SI Appendix*, Table S1). The roundish e type shows a reversed pattern with a core of dense material and a more diffuse material at the periphery (Fig. 1 *A*, *e* and *SI Appendix*, Table S1). Finally, the roundish f type is characterized by a well-developed network of nonmembranous fibrils resembling a ball of wool (Fig. 1 *A*, *f* and *SI Appendix*, Table S1). In addition, we observed that cores of c types were similar to intraluminal contents of b, d, and e types (*SI Appendix*, Fig. S3).

Fine Two-Dimensional/Three-Dimensional Morphological Features of Pigment Organelles Revealed by HPF. The limiting membrane of pigmented organelles at various maturation stages show the typical 8-nm-thick bilayer structure (Fig. 1 *B*, *Inset*, arrowheads). All pigment organelle types could harbor ILVs (shown for five organelles in Fig. 1 *C*, *E*, and *F*, arrows and *SI Appendix*, Fig. S4 *A–C*) and tubulating membranes (shown for three organelles in Fig. 1 *D*, *G*, and *H*, arrows and *SI Appendix*, Fig. S4*D*). Membranes of ILVs within pigment organelles were also well preserved (Fig. 1 *C*, *Inset*, white arrowheads), and some were attached or at least closely associated with the limiting membrane of pigment organelles (Fig. 1 C, *Inset*, E, and F, *Inset*). One particular feature of these ILVs was the presence of a fibrillary material attached to their luminal face (Fig. 1 *C*, *E*, and *F*, black arrowheads). Electron tomography (ET) revealed in three dimensions that those fibrils displayed a sheet-like structure expanding from the ILV surface into the pigment organelle lumen (Fig. 1 *F*, *Inset*, arrowhead and Movie S1), similar to melanosomes (28). Tubules in continuity with pigment organelle membranes were also observed protruding into the cytoplasm (Fig. 1 *D*, *G* and *H*, arrows). In Fig. 1*D*, the content within the tubule is denser than that of pigment organelles, indicating that it might carry substantial amounts of materials either from or to pigment organelles. In Fig. 1 *G* and *H*, ET revealed a tubule

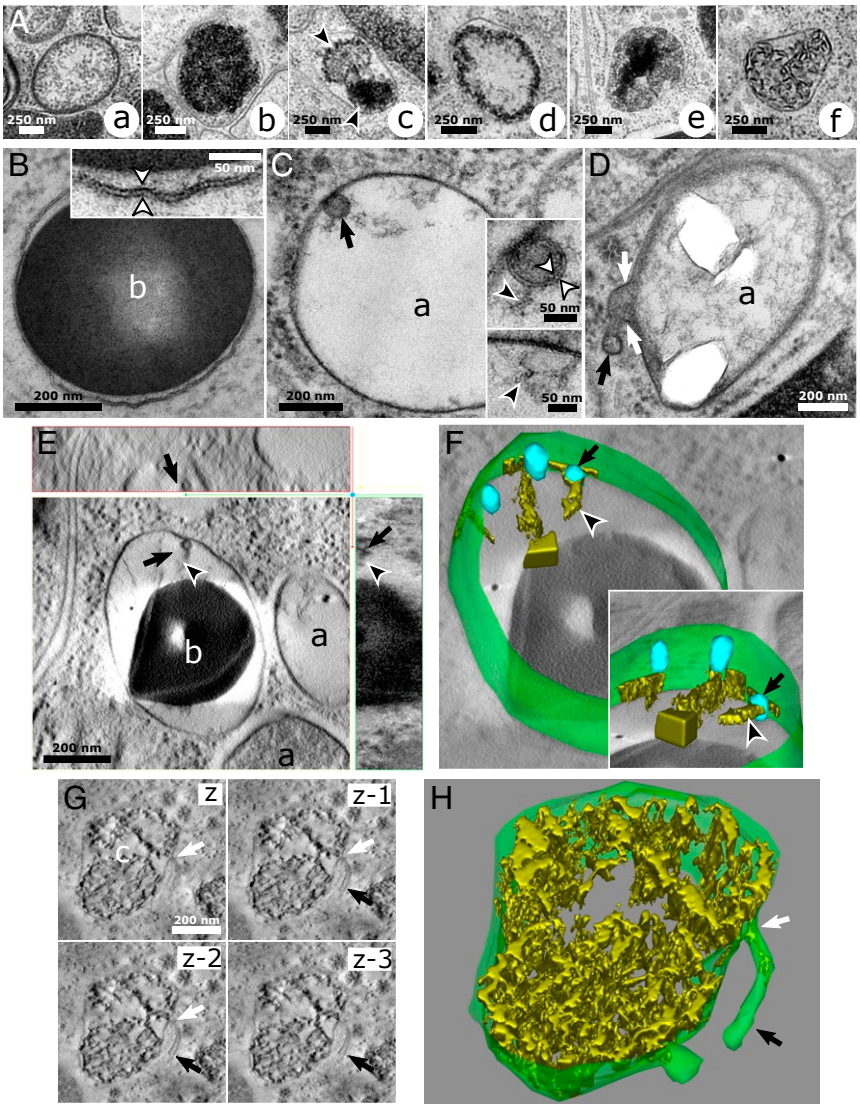

Fig. 1. HPF reveals fine ultrastructural features relating pigment organelles of crab spiders to LROs. (*A*) Pigment organelles are categorized into six types labeled *A*, *a* to *A*, *f* according to the morphology of their luminal content. (*B*) A b-type pigment organelle. (*Inset*) Double-leaflet structure (white arrowheads) of the limiting membrane. (*C*) An a-type pigment organelle containing an ILV (black arrow). (*Upper Inset*) Double-leaflet structure (white arrowheads) of the ILV membrane bearing fibrils (black arrowhead). (*Lower Inset*) Similar fibrils (black arrowhead) are attached to the limiting membrane. (*D*) A membrane tubulation (black arrow) in continuity (white arrows) with the limiting membrane of an a-type pigment organelle. (*E*) Electron tomogram slices showing a fibril-bearing (black arrowheads) ILV (black arrows) attached to the limiting membrane of a maturing b-type pigment organelle. (*Upper*) The *xz* plane. (*Lower Left*) The *xy* plane. (*Lower Right*) The *yz* plane. (*F*) A 3D reconstruction of the pigment organelle depicted in *D* showing its limiting membrane (green), ILVs (blue; black arrow), and fibrils (gold; black arrowhead). (*Inset*) Rotated view showing the sheet-like structure of fibrils (Movie S1). (*G*) Electron tomogram slices in the *z* direction of a c-type pigment organelle bearing a membrane tubulation (black arrows) with a constricted neck (white arrows). *z* to *z-3*, four successive *xy* planes in the *z* direction. (*H*) A 3D reconstruction of the pigment organelle depicted in *G* showing the continuity between its limiting membrane and two tubules (Movie S2). a, a-type pigment organelle; b, b-type pigment organelle.

(Movie S2) whose end was not connected to any other organelles (black arrows) and with a very narrow connection to the pigment organelle (white arrows). Although we did not observe other tubules in three dimensions, this particular occurrence and those observed in two dimensions (Fig. 1*D*) demonstrate that tubulation can exist in the crab spider system.

Analysis of Metals in Pigment Organelles by Correlative SXRF–Scanning Transmission EM. Metals are regulated within the cell by LROs (26), and they can thus serve as cellular markers of this organelle family in the absence of classic markers of model systems. Hence, we looked for metals within pigment organelles of crab spiders using SXRF. To study metal deposition in relation to the variety of pigment organelle types, we performed SXRF analysis on a yellow spider after 1 wk of bleaching (Fig. 2), as well as two fully white and yellow spiders (*SI Appendix*, Fig. S5). We expected metals, if any, to be distributed locally and at low concentrations. To gain structural information during SXRF mapping, we took advantage of the presence of exogenously applied osmium (Os; used as a fixative during freeze substitution) to delineate structures at different scales, such as cuticle and cell layers (Fig. 2*A*), pigment cells (apposed to the cuticle) (Fig. 2*B*), and organelles (Os-positive cytosolic structures) (Fig. 2 *B* and *C*, arrowheads). Native metal mapping reveals that those Os-positive structures differentially accumulate zinc (Zn), calcium (Ca), and to some degree, cobalt (Co) (Fig. 2 *C*, *Insets* and *SI Appendix*, Fig. S5). The correlative SXRF–scanning transmission electron microscopy (STEM) approach confirms

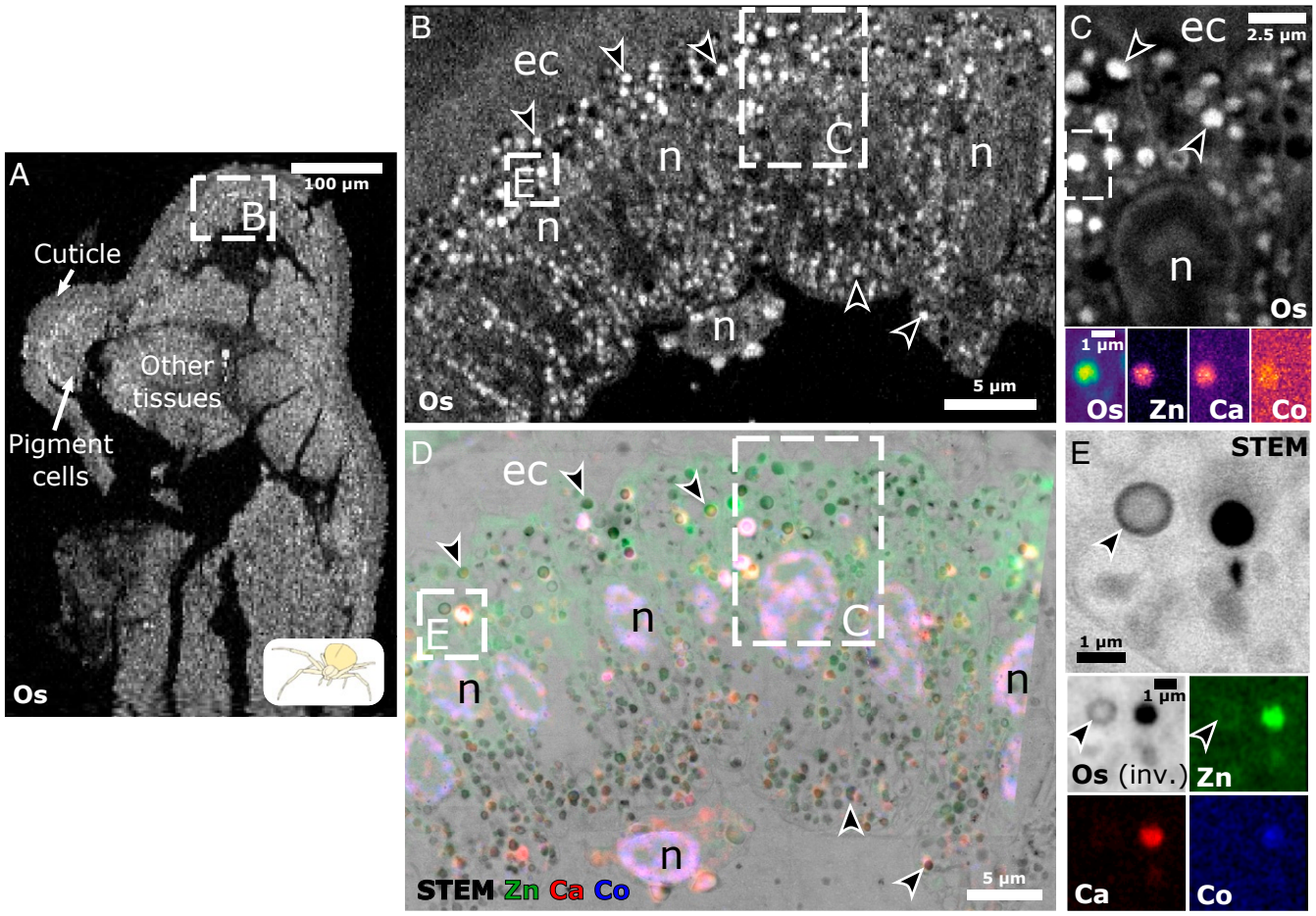

Fig. 2. Correlative SXRF and STEM reveal metal accumulation in pigment organelles. (*A–C*) Hierarchical length-scale SXRF of Os (white) enables the structural mapping of high-pressure frozen integuments, from tissues down to subcellular organelles. (*A*) Pixel size, 2 µm/px. Integration time, 10 ms. (*B*) Zoomed-in view of the region depicted in *A*. Pixel size, 500 nm/px. Integration time, 20 ms. (*C*) Zoomed-in view of the upper region depicted in *B*. Pixel size, 50 nm/px. Integration time, 20 ms. (*Insets*) Os, Zn, Ca, and Co colocalize to discrete structures in the region depicted in *C*. Pixel size, 50 nm/px. Integration times, 20 ms (Os) and 300 ms (Zn, Ca, and Co). (*D*) Correlative SXRF–STEM of the region depicted in *B*. SXRF pixel size, 200 nm/px. Integration time, 200 ms. ec, endocuticle; n, nucleus. (*E*) STEM and SXRF (Os in black) of the lower region depicted in *B* and *D* show similar structures (e.g., black arrowheads). (*Insets*) Os, Zn, Ca, and Co signals of the same area imaged by STEM. inv., inverted colors.

that Os-positive structures correspond to the dense intraluminal material of pigment organelles seen by EM (Fig. 2*E*, arrowheads). SXRF mapping at 50 nm/pixel (px) even recapitulates the heterogeneous intraluminal organization between and within pigment organelles (Fig. 2*E*, arrowheads). Hence, mapping Os is an interesting alternative to visualize pigment organelles at various stages in case ultrastructural information is not readily available. Finally, by applying this correlative approach to native metals, we unambiguously showed that pigment organelles are the main cytosolic sites of metal deposition in pigment cells (Fig. 2 *D* and *E*). A comparative analysis of white and yellow spiders by correlative SXRF–STEM further shows that metal accumulations in pigment organelle correlate with coloration (*SI Appendix*, Fig. S5 *A* and *B*). It further demonstrates that mature pigment organelles (b types) are the preferred sites of Zn, Ca, and Co depositions, while metal concentrations are markedly lower in a, d, e, and f types (*SI Appendix*, Fig. S5 *C–G*; *SI Appendix*, *SI Results* has a detailed description).

Intracellular Origin of Pigment Organelles. We next investigated the intracellular processes underlying pigment organelle biogenesis, maturation, and degradation. Under the hypothesis that pigment organelles are LROs, both endosomal and secretory systems (i.e., Golgi and post-Golgi compartments) could contribute to their biogenesis (3). Therefore, we looked for ultrastructural evidence of either a Golgi or an endosomal origin of pigment organelles.

We spotted on several occasions elongated, swollen, and stacked tubulosaccular complexes that were in the close vicinity of a-type pigment organelles (nine tubulosaccular complexes from seven cells are shown in Fig. 3*A* and *SI Appendix*, Fig. S6, asterisks). Those complexes were mainly found in the perinuclear region and sometimes in association with centrioles (*SI Appendix*, Fig. S6). Fig. 3 *A–C* shows that these complexes are associated with endosomes (white arrow) and microtubules (black arrowheads), as well as free tubules and coated and uncoated vesicles (white arrowheads), suggesting that they are regions of intense membrane trafficking. Strikingly, swollen cisternae of these complexes resembled the most electron-lucent a types (Fig. 3*A* vs. Fig. 3 *B* and *C*). We next performed three-dimensional (3D) analyses by ET to further unravel the unique morphology of these complexes and their relationships with other compartments. Fig. 3*D* reveals that tubulosaccular complexes are composed of distinct side-by-side compartments, each being a complex network of membranes forming tubules, saccules, and elongated structures (Fig. 3*E* and

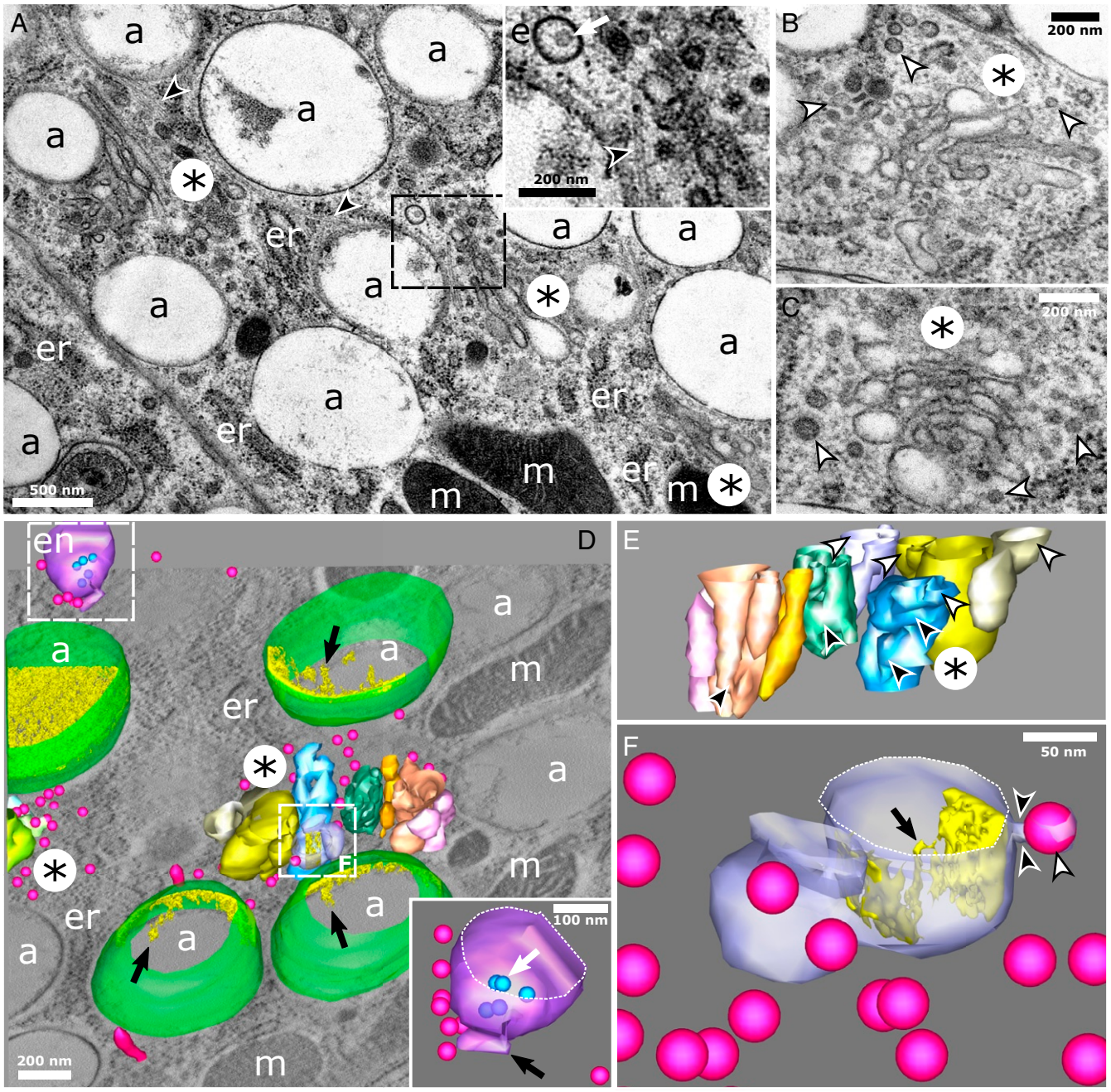

Fig. 3. Maturing a-type pigment organelles are associated with tubulosaccular complexes in regions enriched in endosomes, vesicles, and tubular carriers. (*A*–*E*) Tubulosaccular complexes (asterisks) are in close vicinity of a-type pigment organelles. (*A*, *Inset*) Zoomed-in view of an endosome (displaying an ILV; white arrow), vesicles, and microtubules (black arrowhead). (*B* and *C*) Tubulosaccular complexes showing swollen structures (asterisks) and numerous free coated and uncoated vesicles (white arrowheads). (*D*) A 3D reconstruction of a tubulosaccular region showing a-type pigment organelles (membrane in green and intraluminal fibrils in yellow), vesicles and tubules (fuchsia), endosome (purple membrane and blue ILVs), and tubulosaccular complexes composed of side-by-side compartments (different colors). Part of a second tubulosaccular complex is seen on the left, surrounded by vesicles. Redundant structures are not modeled for clarity. Movie S3 shows a more exhaustive segmentation. (*Inset*) Close-up view of the endosome (Movie S4) displaying ILVs (blue; white arrow) and a tubule (black arrow). (*E*) Close-up view of the tubulosaccular complex at the center of *D*. The view angle is rotated to reveal the different side-by-side compartments (distinguished by different colors). Each of these compartments is made of subcompartments with tubular connections (black arrowheads) and swollen cisternae (white arrowheads). (*F*) Details of one compartment from the main tubulosaccular complex in *D* showing the constricted neck (black arrowheads) of a budding vesicle (white arrowhead) and intraluminal materials (gold) forming fibril-like structures (black arrow) attached to the limiting membrane. a, a-type pigment organelle; en, endosome; er, endoplasmic reticulum; m, mitochondria.

Movie S3). Free vesicles are typically observed in between these compartments (Fig. 3*D*). A budding profile observed in Fig. 3*F*, arrowheads, suggests that tubulosaccular complexes may be one source of free vesicles. The presence of an endosome with typical ILVs and an attached tubule (Fig. 3 *D*, *Inset*, white and black arrows, respectively, and Movie S4) indicates that endosomal compartments could also generate some of the tubular and vesicular carriers observed in this region. Moreover, Fig. 3*D* shows that tubulosaccular complexes are surrounded by a-type pigment organelles with different densities of

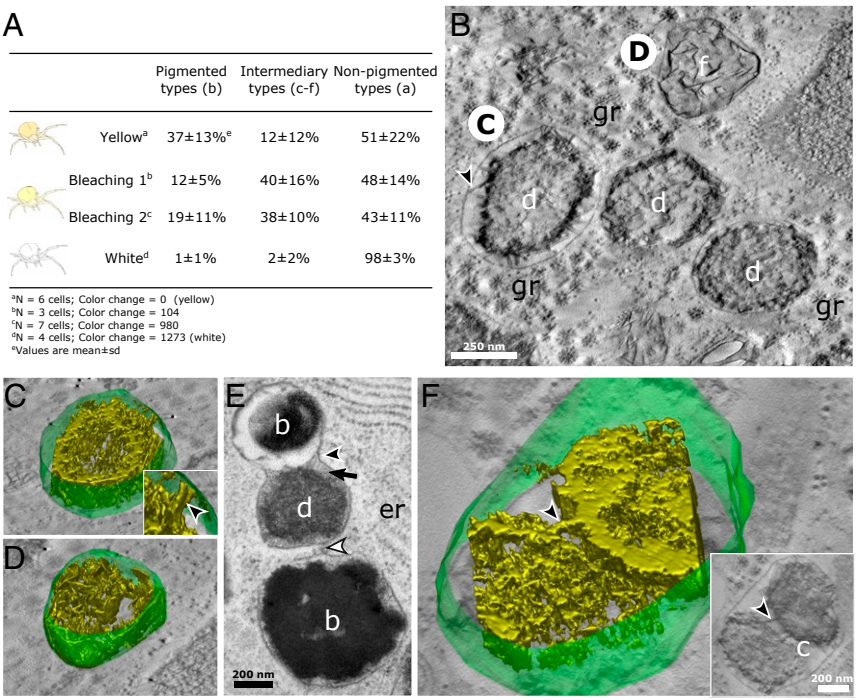

Fig. 4. Degradation stages of pigment organelles during bleaching of crab spiders. (*A*) Proportions of pigment organelle types within pigment cells according to bleaching status. The yellow spider had not undergone bleaching, whereas the white spider was fully bleached. *Materials and Methods* discusses the color change index. *SI Appendix*, Fig. S8 shows a ternary plot visualization of those data. (*B*) Electron tomogram slice in the *xy* plane of d and f types in a bleaching spider. The black arrowhead indicates the structure linking the internal content of a d type to its limiting membrane. (*C* and *D*) A 3D reconstructions of the limiting membrane (green) and the luminal content (isosurface rendering; gold) of two pigment organelles depicted in *B*. (*C*, *Inset*) Zoomed-in view showing a pillar-like structure (black arrowhead) linking the luminal content to the limiting membrane (Movies S5 and S6). (*E*) Continuity (black arrowhead) and close vicinity (white arrowhead) of limiting membranes suggest the heterotypic fusion events between different pigment organelle types. (*F*) A 3D reconstruction of a c-type cluster containing two pigment cores of different nature connected by a pillar-like structure (black arrowheads) (Movie S7). (*Inset*) Electron tomogram slice in the *xy* plane showing connexions between pigment cores (black arrowhead). b, b-type pigment organelle; c, c-type type pigment organelle; d, d-type pigment organelle; f, f-type pigment organelle; gr, glycogen rosette; er, endoplasmic reticulum.

intraluminal fibrils, which suggests that a types mature in this part of the cell. Multiple vesicles can be seen in the vicinity of a types, particularly at the interface with tubulosaccular complexes (Fig. 3*D*). Strikingly, the swollen compartment from the tubulosaccular complex harboring an attached vesicle contains elongated fibrils that emanate from the luminal face of the limiting membrane (Fig. 3*F*, black arrow), which is reminiscent of fibrils in a types.

The rather limited size of swollen compartments in tubulosaccular complexes questions how a types scales up to a micrometer and sometimes even more (Fig. 3*A*). We therefore looked for ultrastructural markers of fusion events implicating pigment organelle precursors. We found many vesicles in the vicinity of tubulosaccular complexes and a types, although very few were directly attached to their membranes (Fig. 3). By contrast, we observed several homotypic fusion events between a types, closely associated with microtubules (*SI Appendix*, Fig. S7). However, we cannot exclude that those observations correspond to fission rather than fusion events. We reason that fission events of such big organelles would constrain their morphology, leading to their deformation near fission sites. Considering the relatively undisturbed aspect of limiting membranes, especially the absence of a constricted neck (*SI Appendix*, Fig. S7 *A* and *C*), fusion events seem more likely.

Intracellular Degradation of Pigment Organelles. We were next interested in how c to f types were related to each other, hypothesizing that they represented catabolic stages of pigment organelle during bleaching rather than anabolic stages of the pigmentation process (i.e., intermediates between a-type precursors and mature b types). To test this hypothesis, we captured yellow crab spiders, measured their body coloration, and let them bleach over time. Each spider was processed for high pressure freezing and freeze substitution (HPF-FS) and transmission electron microscopy (TEM) analysis, representing a different state of bleaching (Fig. 4*A*). Under the hypothesis that c to f types are anabolic stages, we would expect them to occur mostly in yellow spiders and less in bleaching ones. Conversely, if they represent catabolic types, they should increase upon bleaching and vanish in fully white spiders (Fig. 4*A*). We found that c, d, f, and e types (altogether referred to as intermediary types) were more abundant in bleaching spiders than in unbleached (i.e., yellow spiders; dominated by mature b types) and fully bleached (i.e., white spiders; dominated by a-type precursors) spiders (Fig. 4*A* and *SI Appendix*, Table S1). These results indicate that c, d, f, and e types are transient organelles of the bleaching process rather than intermediary anabolic stages.

We then investigated the ultrastructure of catabolic stages using two-dimensional (2D) and 3D EM looking for markers of degradation. Fig. 4 *B–D* shows that intraluminal materials of d and f types are similar to each other, forming a core of dense material that extends in three dimensions and that connects the limiting membrane via pillar-like structures (Fig. 4 *C*, *Inset*, arrowhead and Movie S5). It suggests that f types, whose fibrils are intertwined sheets (Movie S6), represent the latest stages of centrifugal degradation, in which only a backbone of sheets remains.

We finally examined the cluster-like c-type pigment organelles. We observe in several instances endosomes, multivesicular bodies, and organelles displaying ultrastructural features of

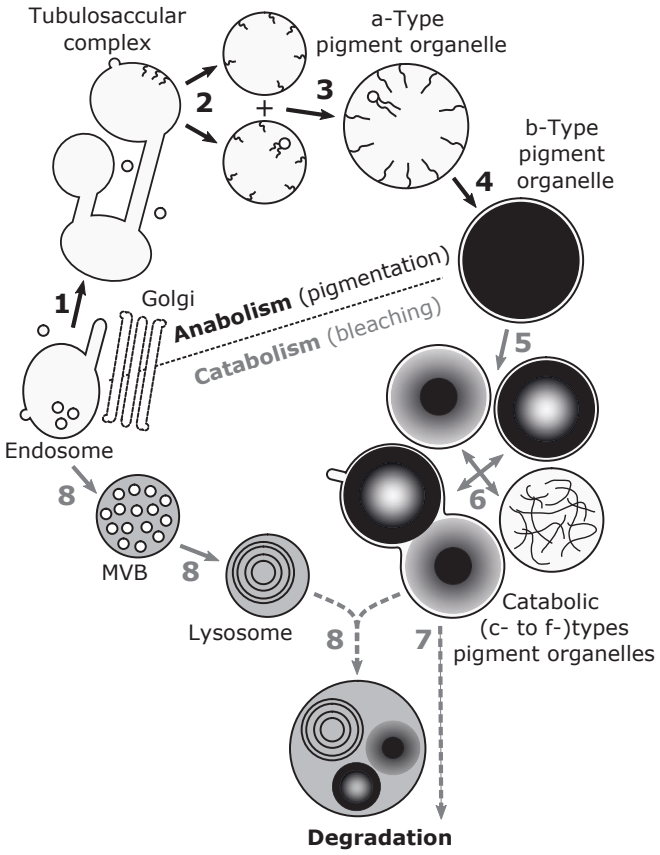

Fig. 5. Working model of the endolysosomal-based pigment turnover leading to reversible color changes of crab spiders. (1) Tubulosaccular complexes originate from endosomes. (2) Tubulosaccular complexes produce pigment organelle precursors (a types) displaying intraluminal fibrils and vesicles. (3) Growth of a types is sustained by homotypic fusion events. (4) Fibril densification and pigment deposition lead to fully pigmented and mature b-type organelles and thus, to yellow coloration. (5) During bleaching, b-type content is variously degraded, leading to catabolic d, e, and f types. (6) Catabolic types cluster together into c types. Catabolic types are degraded by either (7) autocatalytic process or (8) fusion events with lytic compartments, such as lysosomes that also derive from endosomes through multivesicular bodies (MVBs). The hypothetical nature of the last two steps is represented by dotted lines.

lysosomes in the vicinity of c to f types (for example, seven lysosomal organelles with pigment-like materials in their lumen are shown in *SI Appendix*, Fig. S9). *SI Appendix*, Fig. S3*D* shows a typical c-type cluster of five pigment organelles enclosed within a single limiting membrane. We observe in Fig. 4*E* a clear fusion event between two b and d types with continuous limiting membranes but with their respective lumens that have not mixed together yet (Fig. 4*E*, black arrowhead). Furthermore, a membrane extension seems to connect the middle e type with another b type (Fig. 4*E*, white arrowhead). Strikingly, the density and granular aspect of the e-type lumen resemble that of lysosome-like organelles previously described (compare Fig. 4*E*, black arrow and *SI Appendix*, Fig. S9). The 3D reconstruction of a c type reveals that cores of materials are mostly independent of each other (i.e., there is no extent mixing of their contents) (Fig. 4*F*), apart from some bridging regions with a pillar-like structure (Fig. 4*F*, arrowheads and Movie S7). They are reminiscent of the membrane-connecting structures observed in Fig. 4 *C*, *Inset*, suggesting that these bridges are structural remnants of organelles before their incorporation into c types.

To further characterize the bleaching mechanism, we performed analytical chemistry on pigments extracted from spiders at various degrees of bleaching. Such experiments have only been performed on pigment anabolism [i.e., yellowing (18)]. We found that bleaching and yellow spiders only differed by the amount of pigments contained and not by a set of new metabolites (*SI Appendix*, Fig. S10), indicating that pigments are either removed or entirely degraded but are not broken down into new compounds (*SI Appendix* has more details).

Discussion

Pigment Organelles of Crab Spiders Are LROs. Our morphological typology of pigment organelles optimally preserved by HPF matches with that of chemically fixed tissues (10, 19) but also, allowed further insights into their fine morphological details. The combination of nanoscale 2D/3D multimodal imaging techniques allowed us to observe features common to melanosomes, including ILVs, sheet-like fibrils showing analogies with physiological amyloids (28), and Zn/Ca accumulation (34). Other studies described ILVs and metals in pheomelanosomes (35, 36) and pterinosomes (37, 38), as well as various metals in insect ommochromasomes (39–41). These ultrastructural and chemical characteristics are shared by LROs independently of their nature and function (5, 26, 42); they hence associate pigment organelles of crab spiders with LROs.

Pigment Organelles of Crab Spiders Likely Share an Endosomal Origin with Those of Other Animals. We observed (unpigmented) a-type precursors of various sizes near tubulosaccular complexes in the perinuclear region comprising endosomal compartments, microtubules, vesicles, and tubules. Intraluminal fibrils similar to those of a types were observed in a tubulosaccular compartment. Altogether, these observations indicate that pigment organelles originate from these tubulosaccular complexes (Fig. 5). It remains unclear whether tubulosaccular organelles are modified Golgi apparatus (they share a stacked structure and numerous free vesicles) or endosomal compartments (they share tubular membranes and intraluminal fibrils). Both organelles are morphologically plastic (43, 44) and localize to the perinuclear region (6). Furthermore, both secretory and endocytic pathways, to which Golgi apparatus and endosomes belong, respectively, are directly involved in the assembly of LROs, although at various steps of biogenesis and maturation processes (3, 5, 45). We favor the hypothesis of an endosomal origin (Fig. 5) for three indirect reasons. First, pigment organelles possess ILVs, which have not been observed in LROs that originate from the Golgi apparatus [e.g., Weibel–Palade bodies (29, 30)]. In line with this argument and to the best of our knowledge, inward budding has not been observed in Golgi compartments either. Second, the numerous striking similarities between pigment organelles and melanosomes, which derive from endosomes, imply that different origins for these two LROs are unlikely. Third, tubulosaccular complexes display morphological analogies with recycling endosomes, which are made of interconnected vesicles/tubules and contribute to melanosome biogenesis and maturation (46). Cytochemical experiments that could distinguish endosomal from Golgi compartments based on their enzymatic activities may clarify the intracellular origin of pigment organelles.

Overall, pigment organelles of crab spiders join the growing list of pigment LROs in distantly related animals, including mammalian melanosomes (3), insect ommochromasomes and pterinosomes (47), fish pterinosomes (48), and lepidopteran riboflavin and uric acid granules (49, 50), as well as snake melanosomes, pterinosomes, and iridosomes (4). Our study therefore provides another piece of evidence that all pigment organelles, from invertebrates to vertebrates, share a common intracellular identity, as postulated 40 y ago by Bagnara et al. (2). In line with recent results (4), our work further suggests that the endosome is the primordial organelle of all pigment LROs (2).

Pigment Organelle Precursors Likely Grow by Homotypic Fusion Events. Two mechanisms could be invoked regarding the growth of pigment organelle precursors (a types): 1) numerous fusion events with vesicular and tubular carriers and 2) homotypic fusion events between early a types. Although large numbers of free vesicles and tubules were spotted in the vicinity of tubulosaccular complexes and a types, we did not observe many of these carriers attached to the limiting membrane of pigment organelle precursors. On the contrary, homotypic fusion events, likely driven by microtubules, between a types were more readily observed, indicating that these events are more frequent and thus, predominant (Fig. 5).

Intracellular Mechanisms of Bleaching in Crab Spiders in Relation to the Endolysosomal System. Based on the morphological similarities between catabolic types, their transient accumulation in bleaching spiders, and the presence of the same metals but at lower concentrations, we suggest that d to f types represent sequential degradative stages of mature b types, culminating with their fusions into c types (Fig. 5). Based on our data, we cannot rank d to f types relative to each other (Fig. 5). They might represent transient states of pigment degradation or parallel catabolic pathways. Further studies are required to disentangle those two hypotheses. The fusion process between pigment organelles into c types might be facilitated by the accumulation of Ca^{2+} since this ion is known to activate fusion of endolysosomal organelles (51). We note that except for some interconnections between the pigment core in c types, their contents remain largely independent from each other and do not mix. Since there is a single limiting membrane, we hypothesize that the rigid nature of pigment cores, as observed in melanosomes and melanocores, impedes their mixing despite having similar biochemistry. Phase separation might also provide an explanation for this absence of mixing, although there are no data to support this hypothesis, either in this ommochrome system or in melanin systems (52). Further investigations are required to characterize the mechanisms and functions of pigment cores remaining unmixed in c types.

How cells handle pigment LRO degradation intracellularly is a key question to understand bleaching of animals. Intracellular removal of pigments is classically mediated by three nonexclusive canonical mechanisms, namely secretion, autophagy, and lysosomal degradation. Here, we focus on the last one (but *SI Appendix* has further discussions of the two others).

For melanosomes, lytic activities were proposed to occur in two ways (8). First, lytic enzymes are delivered to melanosomes by their fusion with bona fide lysosome, the degradative organelle of the late endosomal pathway. Second, lytic enzymes that are intrinsically associated with melanosomes because of their lysosomal character get activated. In our analysis of bleaching crab spiders, we observed in several occasions catabolic pigment LROs with a dense granular lumen similar to multivesicular bodies and lysosomes, as well as catabolic pigment LROs fused with organelles morphologically similar to lysosomes. Lysosomes might hence potentially deliver their lytic content to pigment LROs (Fig. 5). The LRO identity of pigment organelles might facilitate their fusion with lysosomes by harboring endolysosomal fusion machineries (53), similarly to premelanosomes that exchange materials with lysosomes through kiss and run interaction thanks to FYVE finger-containing phosphoinositide kinase (PIKfyve) activity (54). Validation of lysosomal identity and fusion will require additional experimentation beyond the scope of this study. The fact that no new metabolites seem to be formed during catabolism of pigments is consistent with our hypothesis that a classical lysosomal mechanism is involved during bleaching, which does not require specific metabolic pathways and thus, no formation of new catabolic compounds (*SI Appendix* has further discussion on pigment chemistry). However, since the number of samples used in the analytical chemistry experiment is limited and because the exact identity of some ommochrome-like compounds is missing, further experiments focusing on the chemistry of bleaching are warranted.

We also noted that catabolic d, e, and f types have nearly the same size as fully pigmented b types and that catabolic types do not always show a lysosome-like dense lumen. This indicates that catabolism of b types does not involve extensive addition of membrane and contents, supporting the hypothesis that pigment LROs possess an autocatalytic activity (10) and thus, do not necessarily need to fuse with bona fide lysosomes for degradation (5). Such autocatalytic activity could stem from their lysosomal character, similar to other LROs like cytolytic granules in lymphocytes (55). On the contrary, the larger size of pigment LROs clusters (c types) may imply fusion with lysosomes, leading to further degradation of pigment materials. It also raises the interesting possibility that the autocatalytic activity of c types might serve to degrade other pigment LROs by mimicking the effect of lysosomal fusion and thus, delivering the lytic material of catabolically active pigment organelles to unaltered ones. This contrasts with keratinocytes that accumulate melanosome clusters in white skin. Those clusters are morphologically similar to c types but inactive, serving as pigment storage (52). For now, our data cannot discriminate between the lysosomal fusion and the autocatalytic hypotheses, warranting further investigations on spiders displaying more varied degrees of bleaching.

In addition to lytic pathways, recycling functions of the endolysosomal system should be considered. Endolysosomal organelles, including melanosomes, are known to recycle their content and membrane via tubulations (54, 56–58). We observed tubulations of a c type, indicating that materials are actively recycled from catabolic stages during bleaching. Since metals are less concentrated in d to f types than in b types, it is conceivable that tubules recycle metals for another turn of yellowing, bridging catabolism to anabolism of pigment LROs. Another explanation for membrane tubulation of catabolic types is that after fusing with lysosomes, the latter are reformed from membrane tubulations, similarly to the lysosomal cycle described in other systems (59). In any case, membrane-loss by tubulation could explain why c types are less big than what would be expected if they solely resulted from organelle fusion.

The presence of all pigment organelle types in yellow and bleaching spiders indicates that their anabolism and catabolism proceed simultaneously within the same cell, highlighting the great metabolic turnover of pigments within pigment cells (Fig. 5) (10). The numerous glycogen rosettes, mitochondria, and lipid droplets observed in our electron micrographs and tomograms may be the fuel or the way to store energy from degraded pigments for another yellowing/bleaching cycle. Interestingly, glucose transporters have been shown to be involved in melanosome maturation (60), a process that might also be required for the yellowing of crab spiders after their bleaching. Further analysis on the link between glycogen content and coloration is warranted to test this hypothesis.

Overall, our results support the idea that pigment cells bleach via the in situ degradation of pigment LROs, which involves the continuous remodeling of both pigment organelle contents and membranes, presumably via lytic and recycling functions of the endolysosomal system. While our data provide some support to a nonautophagic process (*SI Appendix*), we cannot exclude its involvement during bleaching, and thus, further investigations are warranted. Similarly, our identification of organelle types based on ultrastructural features and metals would gain from being validated by complementary markers (e.g., Ras-related in brain [Rab] antibodies) and endocytic tracers (e.g., lysotracker), which are available in classical cell systems but that remain to be developed for spiders.

Within-Cell Turnover of Pigments: Physiological and Evolutionary Implications. We propose that, in the context of morphological color changes, the endolysosomal system is adapted and fully functionalized not only to produce and store pigments but also, to catabolize them without requiring cell death or phagocytosis (Fig. 5). Such a hypothesis of intracellular pigment turnover has been debated for melanosomes in mammal eyes (8, 11). It is still unclear whether melanosomes can be degraded intracellularly, even by other cells than melanocytes (8, 12, 52, 61, 62). Most degradative compartments containing melanin are autophagic and occur in pathological contexts, such as melanoma and vitiligo (8). Our results on pigment LROs of crab spiders imply that lysosomal degradation might exist for other pigments produced by the endolysosomal system. Such within-cell turnover of pigment organelles might allow organisms either to display phenotypic plasticity (e.g., slow reversible color changes) (Fig. 5) or to cope with adverse conditions (e.g., photodegradation by free radicals or heavy metals) while maintaining cell functions. Because pigment LROs are ubiquitous in animals (this study and refs. 3 and 4), it further implies that the fundamental anabolic and catabolic functions of the endolysosomal system have been widely co-opted during animal evolution to handle pigment–light interactions.

The fascinating color-changing ability of the nonmodel crab spider is thus in a unique position to provide key physiological understanding, which is otherwise very difficult to obtain, of LRO catabolism in the maintenance of light screening by human ocular melanosomes (8, 11).

Materials and Methods

Specimen Sampling. *Misumena vatia* (Clerck, 1757) crab spiders were collected in fields around the city of Tours, France during the summers of 2018 and 2019. White and yellow individuals were sampled on plants harboring white and yellow flowers, respectively. They were kept individually in plastic vials no more than a week before dissection and fixation to avoid pigmentation loss.

To trigger bleaching of yellow spiders, individuals were left in plastic boxes covered with white cardboard and maintained indoors at room temperature. Spiders were fed once a week, at least 2 d before being further processed.

Integument Fixation and Embedding. Crab spiders were killed and fixed one at a time. For each individual, a few millimeters squared piece of integument was dissected from the opistosoma in Mg-containing Ringer's solution supplemented with 2.2% glucose for isotonicity. HPF was performed with HPM100 (Leica Microsystems) or HPM Live μ (CryoCapCell) in 100% fetal bovine serum (FBS) serving as cryoprotectant. Freeze substitution was performed with AFS2 (Leica Microsystems) in anhydrous acetone containing 2% H_2O/1% OsO_4. Samples were included in Durcupan AMC (EMS).

ET. Sections (300 nm) were cut with the ultramicrotome UCT (Leica Microsystems). Random labeling was performed on both section sides with gold nanoparticles PAG 15 nm (AZU; Utrecht University). Single-tilt series with an angular range of −60° to +60° with 1° increments were imaged at 200 kV using the transmission electron microscope Tecnai G2 (Thermo Fischer Scientific) equipped with a TemCam-F416 4k CMOS camera (TVIPS) controlled by EM-Tools software (TVIPS). Alignment of projection images and tomogram computing (reconstruction-weighted back projection) were performed with Etomo in IMOD software (63). Modelization was performed by manual contouring with 3dmod in IMOD software (64).

SXRF. Sections of 500-nm thickness were cut with the microtome RM2265 (Leica Microsystems). They were deposited at the surface of distilled water drops lying on silicon nitride membranes (membrane size: 1 × 1 mm, membrane thickness: 1 μm; Silson). Membranes were quickly dried for a few seconds at 60°C on a hot plate. Frames were glued on plastic washers to mount them on holders for SXRF.

Hierarchical length-scale SXRF imaging was performed at the Nanoscopium beamline of Synchrotron SOLEIL at Gif-sur-Yvette, France. Multielemental maps were acquired by fast continuous raster scanning using the FLYSCAN scheme (65) with pixel sizes from 2 μm down to 50 nm and with exposure times from 300 to 10 ms per pixel. Full SXRF spectra were recorded for each pixel using two silicon drift detectors (KETEK) placed at ±120° to the beam direction (66). A 10.8-keV photon beam energy was used to excite all native elements from Al to Zn without exciting Os (*SI Appendix*, Fig. S11), which was added as a fixative during FS. The latter was specifically excited for morphological information by changing, on the fly, the beam energy to 11.4 keV.

Endogenous elements (10.8-keV) and Os (11.4-keV) maps were aligned by using DaVis software (LaVision). The following parameters were used: "fill-up empty spaces," "smoothing 2x at 3 px x 3 px," and "deformation with vector field." The Zn signal was retained as a marker for alignment because it presented similar features to Os both in nuclei and in cuticles, which allowed for a meaningful map correlation.

STEM. Frames analyzed by SXRF were removed from plastic washers and were introduced into a custom sample holder crafted to accommodate large silicon nitride frames. Os, without further sample staining, provided enough electron contrast to allow a direct comparison between STEM and SXRF maps. STEM was performed on a 200-kV field emission gun JEM-2200FS (JEOL) equipped with a bright-field STEM detector. A 10-μm condenser aperture was used, and the camera length was set to 60 cm. In these conditions, the beam convergence and collection semi-angles were 6 and 6.6 mrad, respectively. Images were collected at a magnification of x40,000 or x60,000 depending on the experiment (corresponding pixel sizes: 1.04 and 0.69 nm, respectively) using Digiscan II controlled by Digital Micrograph (Gatan). To observe large areas and allow correlative analysis with SXRF images, mosaic STEM images were automatically collected using a laboratory-made script developed in Digital Micrograph.

Correlative SXRF and STEM. Images of the same integument regions were sequentially acquired by SXRF and then by STEM. Correlative imaging was performed using the eC-CLEM plugin (67) in Icy software (68). STEM images and Os (or Zn) maps were set as target and transformed images, respectively. Nonrigid registration was done using natural fiducials markers, such as cuticle edges, nuclei, and sample defects, which were easily and unambiguously observed in Os maps and STEM micrographs.

Image Analysis and Quantification. For color-changing experiments, spiders at different states of bleaching were processed by HPF-FS and TEM. To quantify proportions of pigment organelle types, only spiders showing the best preservation and ultrastructures were retained. Three to seven cells per spider were selected based on their section profile displaying both basal and apical poles and the nucleus. In each cell, pigment organelles were counted and classified based on their ultrastructural morphologies. For most morphological observations, supporting information presents a range of examples to show their variety and variability.

Data Availability. All study data are included in the article and/or supporting information.

ACKNOWLEDGMENTS. We thank Teresita Insausti, Carole Labrousse, Suzanne Rochefort, Maryse Romao, and Thibaut Munsch for their help as well as Michael Marks for his comments on an early version of this manuscript. We acknowledge SOLEIL for provision of synchrotron radiation facilities (Projects 20180104 and 20190205), and we thank Gil Baranton for assistance in using the "Nanoscopium" beamline. We also acknowledge the Multimodal Imaging Centre at Institut Curie Orsay for providing access to the cryo-EM facility and the Cell and Tissue Imaging Platform–PICT-IBiSA (member of France–Bioimaging–ANR-10-INBS-32904) of the UMR144 of Institut Curie for help with EM. The École Normale Supérieure de Lyon and the Project "PHEROAERO" of the Région Centre supported the work of F.F.

1. A. E. Needham, *The Significance of Zoochromes* (Springer-Verlag, 1974), vol. 3.
2. J. T. Bagnara *et al*., Common origin of pigment cells. *Science* **203**, 410–415 (1979).
3. C. Delevoye, M. S. Marks, G. Raposo, Lysosome-related organelles as functional adaptations of the endolysosomal system. *Curr. Opin. Cell Biol.* **59**, 147–158 (2019).
4. A. Ullate-Agote *et al*., Genome mapping of a *LYST* mutation in corn snakes indicates that vertebrate chromatophore vesicles are lysosome-related organelles. *Proc. Natl. Acad. Sci. U.S.A.* **117**, 26307–26317 (2020).
5. S. L. Bowman, J. Bi-Karchin, L. Le, M. S. Marks, The road to lysosome-related organelles: Insights from Hermansky-Pudlak syndrome and other rare diseases. *Traffic* **20**, 404–435 (2019).

6. J. Klumperman, G. Raposo, The complex ultrastructure of the endolysosomal system. *Cold Spring Harb. Perspect. Biol.* **6**, a016857 (2014).
7. F. Figon, J. Casas, Ommochromes in invertebrates: Biochemistry and cell biology. *Biol. Rev. Camb. Philos. Soc.* **94**, 156–183 (2018).
8. J. Borovanský, M. Elleder, Melanosome degradation: Fact or fiction. *Pigment Cell Res.* **16**, 280–286 (2003).
9. E. Candi, R. Schmidt, G. Melino, The cornified envelope: A model of cell death in the skin. *Nat. Rev. Mol. Cell Biol.* **6**, 328–340 (2005).
10. T. C. Insausti, J. Casas, Turnover of pigment granules: Cyclic catabolism and anabolism of ommochromes within epidermal cells. *Tissue Cell* **41**, 421–429 (2009).
11. U. Schraermeyer, Does melanin turnover occur in the eyes of adult vertebrates? *Pigment Cell Res.* **6**, 193–204 (1993).
12. H. Ho, A. K. Ganesan, The pleiotropic roles of autophagy regulators in melanogenesis. *Pigment Cell Melanoma Res.* **24**, 595–604 (2011).
13. N. Otaki, M. Seiji, Degradation of melanosomes by lysosomes. *J. Invest. Dermatol.* **57**, 1–5 (1971).
14. G. Szabó, A. B. Gerald, M. A. Pathak, T. B. Fitzpatrick, Racial differences in the fate of melanosomes in human epidermis. *Nature* **222**, 1081–1082 (1969).
15. J. P. Ebanks *et al*., Epidermal keratinocytes from light vs. dark skin exhibit differential degradation of melanosomes. *J. Investig. Dermatol.* **131**, 1226–1233 (2011).
16. M. Théry, J. Casas, Predator and prey views of spider camouflage. *Nature* **415**, 133 (2002).
17. A. G. Anderson, G. N. Dodson, Colour change ability and its effect on prey capture success in female *Misumenoides formosipes* crab spiders: Colour change and foraging in a crab spider. *Ecol. Entomol.* **40**, 106–113 (2015).
18. A. L. Llandres, F. Figon, J.-P. Christidès, N. Mandon, J. Casas, Environmental and hormonal factors controlling reversible colour change in crab spiders. *J. Exp. Biol.* **216**, 3886–3895 (2013).
19. T. C. Insausti, J. Casas, The functional morphology of color changing in a spider: Development of ommochrome pigment granules. *J. Exp. Biol.* **211**, 780–789 (2008).
20. F. Figon *et al*., Uncyclized xanthommatin is a key ommochrome intermediate in invertebrate coloration. *Insect Biochem. Mol. Biol.* **124**, 103403 (2020).
21. R. Futahashi, R. Kurita, H. Mano, T. Fukatsu, Redox alters yellow dragonflies into red. *Proc. Natl. Acad. Sci.* **109**, 12626–12631 (2012).
22. T. L. Williams *et al*., Dynamic pigmentary and structural coloration within cephalopod chromatophore organs. *Nat. Commun.* **10**, 1004 (2019).
23. F. Figon, J. Casas, I. Ciofini, C. Adamo, Electronic coupling in the reduced state lies at the origin of color changes of ommochromes. *Dye. Pigment.* **185**, 108661 (2021).
24. K. D. L. Umbers, S. A. Fabricant, F. M. Gawryszewski, A. E. Seago, M. E. Herberstein, Reversible colour change in Arthropoda. *Biol. Rev.* **89**, 820–848 (2014).
25. F. Figon, J. Casas, "Morphological and physiological colour changes in the animal kingdom" in *eLS*, John Wiley & Sons Ltd., Ed. (John Wiley & Sons, Ltd., Chichester, United Kingdom, 2018), pp. 1–11.
26. C. E. Blaby-Haas, S. S. Merchant, Lysosome-related organelles as mediators of metal homeostasis. *J. Biol. Chem.* **289**, 28129–28136 (2014).
27. I. Hurbain, M. Romao, P. Bergam, X. Heiligenstein, G. Raposo, "Analyzing lysosome-related organelles by electron microscopy" in *Lysosomes*, K. Öllinger, H. Appelqvist, Eds. (Springer, New York, 2017), vol. 1594, pp. 43–71.
28. I. Hurbain *et al*., Electron tomography of early melanosomes: Implications for melanogenesis and the generation of fibrillar amyloid sheets. *Proc. Natl. Acad. Sci. U.S.A.* **105**, 19726–19731 (2008).
29. K. M. Valentijn, J. A. Valentijn, K. A. Jansen, A. J. Koster, A new look at Weibel-Palade body structure in endothelial cells using electron tomography. *J. Struct. Biol.* **161**, 447–458 (2008).
30. H. L. Zenner, L. M. Collinson, G. Michaux, D. F. Cutler, High-pressure freezing provides insights into Weibel-Palade body biogenesis. *J. Cell Sci.* **120**, 2117–2125 (2007).
31. R. McRae, P. Bagchi, S. Sumalekshmy, C. J. Fahrni. In situ imaging of metals in cells and tissues. *Chem. Rev.* **109**, 4780–4827 (2009).
32. J. Decelle *et al*., Algal remodeling in a ubiquitous planktonic photosymbiosis. *Curr. Biol.* **29**, 968–978 (2019).
33. A. Gal *et al*., Native-state imaging of calcifying and noncalcifying microalgae reveals similarities in their calcium storage organelles. *Proc. Natl. Acad. Sci. U.S.A.* **115**, 11000–11005 (2018).
34. T. Gorniak *et al*., Support and challenges to the melanosomal casing model based on nanoscale distribution of metals within iris melanosomes detected by X-ray fluorescence analysis. *Pigment Cell Melanoma Res.* **27**, 831–834 (2014).
35. K. Jimbow, O. Oikawa, S. Sugiyama, T. Takeuchi, Comparison of eumelanogenesis and pheomelanogenesis in retinal and follicular melanocytes; role of vesiculo-globular bodies in melanosome differentiation. *J. Invest. Dermatol.* **73**, 278–284 (1979).
36. P. Stanka, Ultrastructural study of pigment cells of human red hair. *Cell Tissue Res.* **150**, 167–178 (1974).
37. P. D. Blanchard, R. A. Angus, R. L. Morrison, S. K. Frost-Mason, J. H. Sheetz, Pigments and ultrastructures of pigment cells in xanthic sailfin mollies (*Poecilia latipinna*). *Pigment Cell Res.* **4**, 240–246 (1991).
38. J. R. Shoup, The development of pigment granules in the eyes of wild type and mutant *Drosophila melanogaster*. *J. Cell Biol.* **29**, 223–249 (1966).
39. F. G. Gribakin *et al*., Reduced magnesium content in non-pigmented eyes of the honey bee (*Apis mellifera* L.). *Comp. Biochem. Physiol. Part A Physiol.* **86**, 689–692 (1987).
40. R. H. White, N. A. Michaud, Calcium is a component of ommochrome pigment granules in insect eyes. *Comp. Biochem. Physiol. Part A Physiol.* **65**, 239–242 (1980).
41. K. Y. Ukhanov, Ommochrome pigment granules: A calcium reservoir in the dipteran eyes. *Comp. Biochem. Physiol. Part A Physiol.* **98**, 9–16 (1991).
42. R. Docampo, G. Huang, Acidocalcisomes of eukaryotes. *Curr. Opin. Cell Biol.* **41**, 66–72 (2016).
43. D. P. Hoffman *et al*., Correlative three-dimensional super-resolution and block-face electron microscopy of whole vitreously frozen cells. *Science* **367**, 5357 (2020).
44. A. A. Mironov, I. S. Sesorova, E. V. Seliverstova, G. V. Beznoussenko, Different Golgi ultrastructure across species and tissues: Implications under functional and pathological conditions, and an attempt at classification. *Tissue Cell* **49** (2 part A), 186–201 (2017).
45. A. Patwardhan *et al*., Routing of the RAB6 secretory pathway towards the lysosome related organelle of melanocytes. *Nat. Commun.* **8**, 15835 (2017).
46. C. Delevoye *et al*., AP-1 and KIF13A coordinate endosomal sorting and positioning during melanosome biogenesis. *J. Cell Biol.* **187**, 247–264 (2009).
47. V. Lloyd, M. Ramaswami, H. Krämer, Not just pretty eyes: *Drosophila* eye-colour mutations and lysosomal delivery. *Trends Cell Biol.* **8**, 257–259 (1998).
48. L. Navarro *et al*., DELLAs control plant immune responses by modulating the balance of jasmonic acid and salicylic acid signaling. *Curr. Biol.* **18**, 650–655 (2008).
49. H. Zhang *et al*., Pigmentary analysis of eggs of the silkworm *Bombyx mori*. *J. Insect Physiol.* **101**, 142–150 (2017).
50. H. Zhang *et al*., Bm-muted, orthologous to mouse muted and encoding a subunit of the BLOC-1 complex, is responsible for the otm translucent mutation of the silkworm *Bombyx mori*. *Gene* **629**, 92–100 (2017).
51. P. R. Pryor, B. M. Mullock, N. A. Bright, S. R. Gray, J. P. Luzio, The role of intraorganellar Ca(2+) in late endosome-lysosome heterotypic fusion and in the reformation of lysosomes from hybrid organelles. *J. Cell Biol.* **149**, 1053–1062 (2000).
52. I. Hurbain *et al*., Melanosome distribution in keratinocytes in different skin types: Melanosome clusters are not degradative organelles. *J. Invest. Dermatol.* **138**, 647–656 (2018).
53. J. P. Luzio, S. R. Gray, N. A. Bright, Endosome-lysosome fusion. *Biochem. Soc. Trans.* **38**, 1413–1416 (2010).
54. C. Bissig *et al*., The PIKfyve complex regulates the early melanosome homeostasis required for physiological amyloid formation. *J. Cell Sci.* **132**, jcs229500 (2019).
55. P. J. Peters *et al*., Cytotoxic T lymphocyte granules are secretory lysosomes, containing both perforin and granzymes. *J. Exp. Med.* **173**, 1099–1109 (1991).
56. M. K. Dennis *et al*., BLOC-1 and BLOC-3 regulate VAMP7 cycling to and from melanosomes via distinct tubular transport carriers. *J. Cell Biol.* **214**, 293–308 (2016).
57. C. Bissig, I. Hurbain, G. Raposo, G. van Niel, PIKfyve activity regulates reformation of terminal storage lysosomes from endolysosomes. *Traffic* **18**, 747–757 (2017).
58. L. Ripoll *et al*., Myosin VI and branched actin filaments mediate membrane constriction and fission of melanosomal tubule carriers. *J. Cell Biol.* **217**, 2709–2726 (2018).
59. N. Bright, L. Davis, J. Luzio, Endolysosomes are the principal intracellular sites of acid hydrolase activity. *Curr. Biol.* **26**, 2233–2245 (2016).
60. N. W. Bellono, I. E. Escobar, A. J. Lefkovith, M. S. Marks, E. Oancea, An intracellular anion channel critical for pigmentation. *eLife* **3**, e04543 (2014).
61. D. Murase *et al*., Autophagy has a significant role in determining skin color by regulating melanosome degradation in keratinocytes. *J. Invest. Dermatol.* **133**, 2416–2424 (2013).
62. M. S. Correia *et al*., Melanin transferred to keratinocytes resides in nondegradative endocytic compartments. *J. Invest. Dermatol.* **138**, 637–646 (2018).
63. D. N. Mastronarde, S. R. Held, Automated tilt series alignment and tomographic reconstruction in IMOD. *J. Struct. Biol.* **197**, 102–113 (2017).
64. J. R. Kremer, D. N. Mastronarde, J. R. McIntosh, Computer visualization of three-dimensional image data using IMOD. *J. Struct. Biol.* **116**, 71–76 (1996).
65. K. Medjoubi *et al*., Development of fast parallel multi-technique scanning x-ray imaging at synchrotron soleil. *J. Phys. Conf. Ser.* **463**, 012031 (2013).
66. A. Somogyi *et al*., Optical design and multi-length-scale scanning spectro-microscopy possibilities at the Nanoscopium beamline of Synchrotron Soleil. *J. Synchrotron Radiat.* **22**, 1118–1129 (2015).
67. P. Paul-Gilloteaux *et al*., eC-CLEM: Flexible multidimensional registration software for correlative microscopies. *Nat. Methods* **14**, 102–103 (2017).
68. F. de Chaumont *et al*., Icy: An open bioimage informatics platform for extended reproducible research. *Nat. Methods* **9**, 690–696 (2012).